Very Stable Electron Field Emission from Strontium Titanate Coated Carbon Nanotube Matrices with Low Emission Thresholds

Archana Pandey,[†] Abhishek Prasad,[†] Jason P. Moscatello,[†] Mark Engelhard,[‡] Chongmin Wang,[‡] and Yoke Khin Yap[†,*]

[†]Department of Physics, Michigan Technological University, 118 Fisher Hall, 1400 Townsend Drive, Houghton, Michigan 49931, United States and
[‡]Environmental Molecular Sciences Laboratory, Pacific Northwest National Laboratory, Richland, Washington 99352, United States

ABSTRACT Novel PMMA—STO—CNT matrices were created by opened-tip vertically aligned multiwalled carbon nanotubes (VA-MWCNTs) with conformal coatings of strontium titanate (STO) and poly(methyl methacrylate) (PMMA). Emission threshold of 0.8 V/μm was demonstrated, about 5-fold lower than that of the as-grown VA-MWCNTs. This was obtained after considering the related band structures under the perspective of work functions and tunneling width as a function of the STO thickness. We showed that there is an optimum thickness of STO coatings to effectively reduce the work function of CNTs and yet minimize the tunneling width for electron emissions. Furthermore, simulation and modeling suggest that PMMA—STO—CNT matrices have suppressed screening effects and Coulombs' repulsion forces between electrons in adjacent CNTs, leading to low emission threshold, high emission density, and prolonged emission stability. These findings are important for practical application of VA-MWCNTs in field emission devices, X-ray generation, and wave amplification.

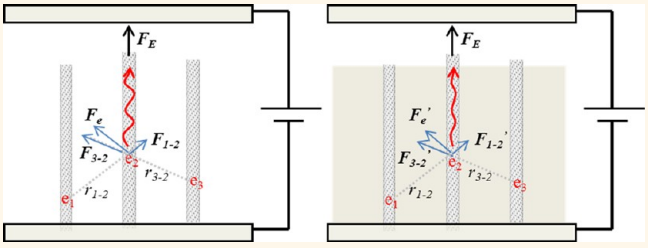

KEYWORDS: carbon nanotubes · strontium titanate · poly(methyl methacrylate) · field emission

Tremendous efforts have been invested to understand electron field emission from carbon nanotubes (CNTs) for more than one decade.[1−7] Most investigations were conducted by demonstrating the low emission threshold field (E_{th}) of CNTs,[1−3] electric field shielding effects of CNT films,[4] device architectures,[5] and mechanical failure of CNTs after excessive current emission.[6,7] However, some of the issues that hindered the realization of reliable applications have not been sufficiently emphasized, including the issue of long-term emission stability.

We have started to understand the basic science behind stable emission current. First, we found that field emission should not be treated by solely considering the quantum tunneling process.[8] Other classical factors such as defect scattering on CNTs and the resulting Joule heating should be considered for stable electron emission. More recently, we showed that opened-tip CNT bundles can improve *both* the emission stability and emission density.[9] On the basis of theoretical simulation, we explained our experimental results by the reduced electric field shielding effect between the CNT bundles. The reduced screening effect has enabled more CNTs to share the workload of emitting electrons and thus reduce the mechanical stress that was generated by Joule heating. These have contributed to better emission stability and higher emission density. Although the emission stability has been improved, the emission threshold, E_{th}, is still high (>2 V/μm). By considering these prior understandings, we have designed a novel STO—PMMA—CNT matrix as the stable electron field emitters with low E_{th}, durable emission stability, and high emission site density.

The PMMA—STO—CNT matrices are referred to as vertically aligned multiwalled CNTs (VA-MWCNTs) that are coated with strontium titanate ($SrTiO_3$ or STO) and poly(methyl

* Address correspondence to ykyap@mtu.edu.

Received for review July 25, 2012 and accepted November 30, 2012.

Published online November 30, 2012
10.1021/nn303351g

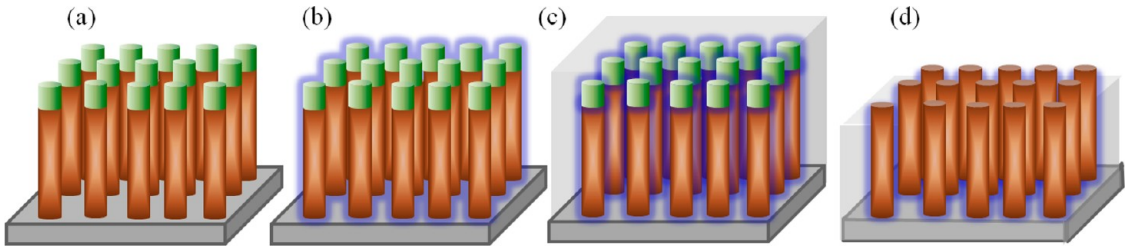

Figure 1. Fabrication scheme of our PMMA–STO–CNT matrices. (a) As-grown VA-MWCNTs with residual Ni catalyst particles at the tips. (b) VA-MWCNTs coated with STO (STO–CNTs), (c) STO–CNTs fully embedded with PMMA, (d) PMMA–STO–CNT matrices with opened STO–CNT tips.

methacrylate) (PMMA). The strategies behind the design of our PMMA–STO–CNT matrices are that STO can reduce *both* the work function of CNTs and screening effect between CNTs. CNTs are known for their high work function ($\Phi_{CNT} \sim 5$ eV).[10] Although the sharp tips and high aspect ratios of CNTs could reduce E_{th}, the screening effects from adjacent CNTs will compensate these advantages. Thus, it is important to reduce the work function and screening effects of the as-grown CNT films *simultaneously*. We think that coating CNTs with $SrTiO_3$ could reduce the work function ($\Phi_{STO} \sim 2.6$ eV)[11] and suppress the screening effect between CNTs due to the high dielectric constant of STO ($k \sim$ as high as 475).[12] Although reduced E_{th} of CNTs was reported for various wide band gap materials,[13−16] the improvement was explained by the lower work function of the coatings. There was no evaluation on the effect of high dielectric constant of these coatings and the long-term emission stability of the emitters as well as the tunneling barriers created by the insulating dielectric.

RESULTS AND DISCUSSION

Here we show that the controlled coating of $SrTiO_3$ can simultaneously reduce the E_{th} of our VA-MWCNTs and enhance the emission density and stability. Furthermore, we can locally open the $SrTiO_3$-coated CNT tips after embedding/masking the STO-coated CNTs by PMMA. These PMMA–STO–CNT matrices were shown to have E_{th} of 0.8 V/μm and enhanced emission density. We further detected continuous electron emission for 40 h from the PMMA–STO–CNT matrices without degradation. Our results clarify that the function of $SrTiO_3$ coating is not just reducing the work function of CNTs. Instead, the high dielectric constant of $SrTiO_3$ coating could have minimized the screening effects between adjacent CNTs without the need of lithograph-based patterned growth. These results were discussed by theoretical simulation and hypothetical modeling. The fabrication scheme of our PMMA–STO–CNT matrices is summarized in Figure 1.

Figure 2a shows the SEM image of the as-grown VA-MWCNTs. The diameters of these CNTs are 30–50 nm, and their lengths are ~4 μm. The appearance of the CNTs in the STO–CNT sample, as shown in Figure 2b, is blurred and larger in diameter, indicating successful coating of the insulating $SrTiO_3$ that caused the charging effect in SEM. Figure 2c shows the typical morphology at the top surface of PMMA–STO–CNT matrices. Despite the charging effect on PMMA under SEM, the opened tips of CNTs can still be detected. Figure 2d–f shows the Raman spectra of as-grown, STO–CNT, and PMMA–STO–CNT samples, respectively. For all samples, the graphitic (G) and defective (D) Raman bands are detected, indicating that the laser-induced Raman scattering of CNTs occurred on all samples. The G and D bands represent the zone center phonons of E_{2g} symmetry and the *K*-point phonons of A_{1g} symmetry of the VA-MWCNTs, respectively.[17] The intensity ratio (I_G/I_D) for all samples (~0.70 ± 0.1 to 0.88 ± 0.1) and their peak positions (G ~ 1586 ± 0.1 cm^{-1} and D ~ 1330 ± 0.2 cm^{-1}) are within the measurement deviation between samples, indicating similar structural properties of the VA-MWCNTs. The physical appearances of these samples are shown in Figure 2g–i.

XPS spectra of the as-grown sample (Figure 3a) showing the presence of the C_{1s} signal. Figure 3b shows the XPS spectra of the STO–CNT samples. The presence of $SrTiO_3$ is confirmed by the composition Sr/Ti/O ~ 1.0:1.0:3.0. Figure 3c,d shows the TEM images of the as-grown and STO–CNT samples. As shown, the overall thickness of the $SrTiO_3$-coated MWCNT is larger than the typical diameters of our as-grown VA-MWCNTs, consistent with the SEM images in Figure 2a,b.

We first examined the effect of STO coatings on our MWCNTs. A series of STO–CNT samples were prepared with various thicknesses of STO coatings and then tested for their field emission characteristics by measuring their current density (*J*) as a function of applied electric field (*E*). The threshold electric field, E_{th} (applied electric field for generating a current density of 1 μA/cm^2), for each sample was then determined and summarized in Figure 4. As shown, E_{th} reached a minimum when the STO film thickness was ~30–40 nm (as measured from our *in situ* thickness sensor during deposition). Such an observation is interesting and has also been reported by Chakrabarti *et al.* with different explanation.[18] In fact, E_{th} for the as-grown sample without STO coating is ~3.8 V/μm. The E_{th} for the STO–CNT sample coated with 10 nm of $SrTiO_3$ remained unchanged but

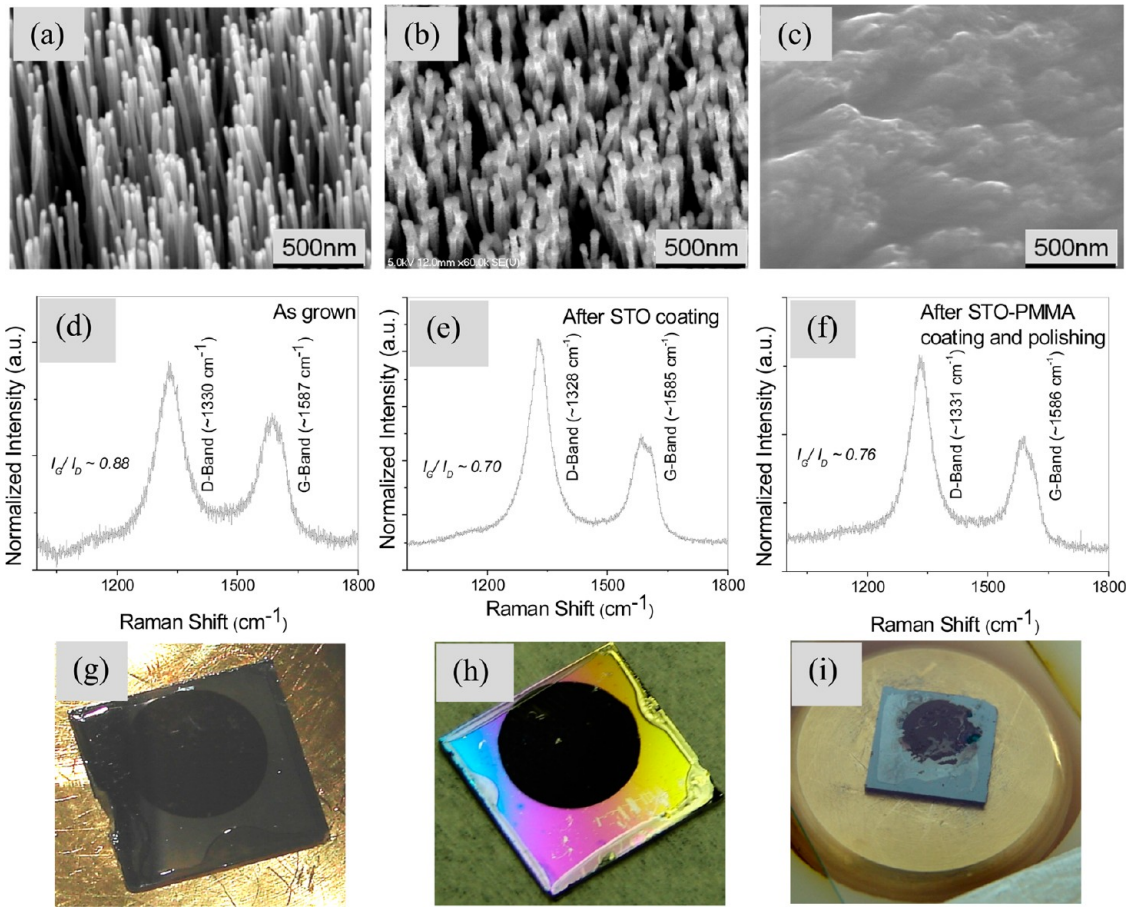

Figure 2. SEM images of the (a) as-grown VA-MWCNTs, (b) STO–CNT sample, and (c) PMMA–STO–CNT matrix. Raman spectra of the (d) as-grown VA-MWCNTs, (e) STO–CNT sample, and (f) PMMA–STO–CNT matrix. Photographs of the (g) as-grown VA-MWCNTs, (h) STO–CNT sample, and (i) PMMA–STO–CNT matrix.

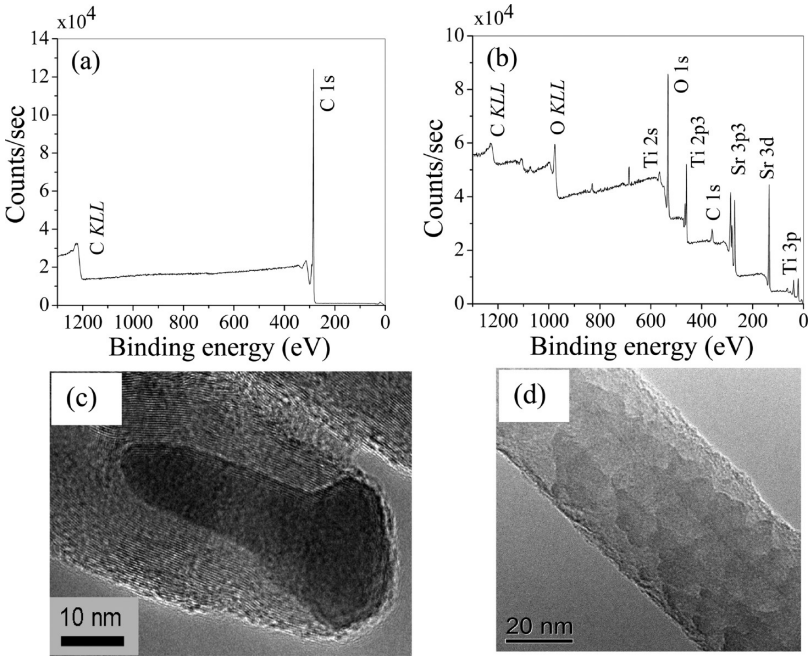

Figure 3. XPS spectra and TEM images of the as-grown (a,c) and $SrTiO_3$-coated (b,d) MWCNTs.

started to reduce only when the thicknesses of $SrTiO_3$ increased to 20–40 nm.

We propose an explanation by referring to the energy band diagram of STO–CNTs. Figure 5 explains

the possible field emission mechanism at the $SrTiO_3$/CNTs interface for the improvement of the field emission from the low work function material coated CNTs. A similar model for the field emission mechanism has been proposed by Schlesser *et al.* for molybdenum emitters coated with diamond.[19] The dependence of E_{th} on the thicknesses of $SrTiO_3$ can be explained by considering work function (Φ_{SrTiO_3}) and band bending of $SrTiO_3$. MWCNTs are semimetallic with a work function (Φ_{CNT}) of ~5 eV, and $SrTiO_3$ is a dielectric with a band gap of ~3.2 eV.[20] When high external electric field is applied, a potential drop of ΔV occurs across $SrTiO_3$ coating, as shown in Figure 5a. Such a band bending effect will lower the vacuum level, valence band maximum, conduction band minimum, and Fermi level across $SrTiO_3$ coating. The mechanism of electron emission can be explained by considering the two-barrier mechanism proposed by Givargizov *et al.*[21] In the first step, electrons are injected from the Fermi level of CNTs to the conduction band of $SrTiO_3$ through a tunneling width W. The injected electron thermalizes to the conduction band minimum of $SrTiO_3$. Finally, the electron is emitted by field emission at the $SrTiO_3$ and vacuum interface. This process effectively lowers the work function by ~2 eV and results in reduced threshold voltage. As interpreted from our results in Figure 4, a minimum thickness of $SrTiO_3$ coating (~15−20 nm) is needed to fully establish Φ_{SrTiO_3}. The reduction of E_{th} will occur only when Φ_{SrTiO_3} is established, probably after a full surface coverage of $SrTiO_3$ on MWCNTs. There seems to be an optimum thickness when E_{th} reaches a minimum. Because of the large dielectric constant, further thickness increase of the $SrTiO_3$ coating will lead to smaller field penetration through the dielectric and reduce the effective electric field between the cathode (CNTs) and the anode, as well as the potential drop ($\Delta V'$) (Figure 5b) across the coating. This will lead to a lower degree of band bending and wider tunneling width (W') and thus reduce the emission current under a same applied electric field. The overall effect is the increase of E_{th} at excessive thickness of $SrTiO_3$ coating.

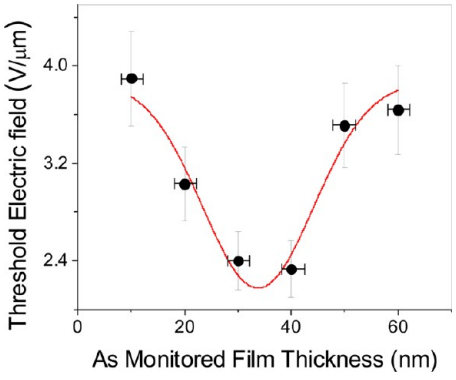

Figure 4. Threshold electric field, E_{th}, for field emission from STO−CNTs as a function of film thickness of the $SrTiO_3$ coatings.

Figure 6a−c shows the relations of current density (J) *versus* electric field (E) of as-grown, STO−CNT, and PMMA−STO−CNT samples, respectively. The Fowler−Nordheim (F−N) equation,[22] $J = A\beta^2E^2\exp(-B\Phi^{3/2}/\beta E)$, is often used to describe electron field emission, where A and B are constants, E is the applied electric field in V cm^{-1}, Φ is the work function of the emitters in eV, and β is the field enhancement factor. Insets of these figures show the corresponding linear F−N plots, which verified that the detected currents are due to quantum tunneling. For this particular set of samples, E_{th} is 3.8, 2.0, and 0.8 V/μm for as-grown, STO−CNT, and PMMA−STO−CNT samples, respectively. This means STO coating (~20 nm thick) can reduce E_{th} of the as-grown VA-MWCNTs as we have discussed in Figures 4 and 5. Furthermore, the combination of conformal PMMA coating of STO−CNT and local removal of the $SrTiO_3$ at the tips of VA-MWCNTs has further reduced the E_{th} of the PMMA−STO−CNT sample.

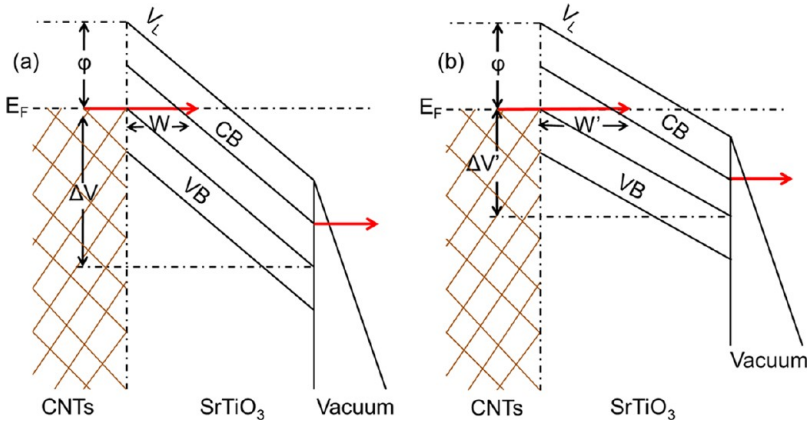

Figure 5. Possible field emission mechanism for STO−CNTs with (a) optimum and (b) excessive thicknesses. As shown, ϕ is the work function of CNTs, V_L is the vacuum level, E_F is the Fermi level, CB and VB are the conduction band and valence band, respectively, while W is the tunneling width of the STO coating. As shown, the band structures of $SrTiO_3$ are bent by the applied electric field and created voltage drops (ΔV and $\Delta V'$) across the $SrTiO_3$ layer.

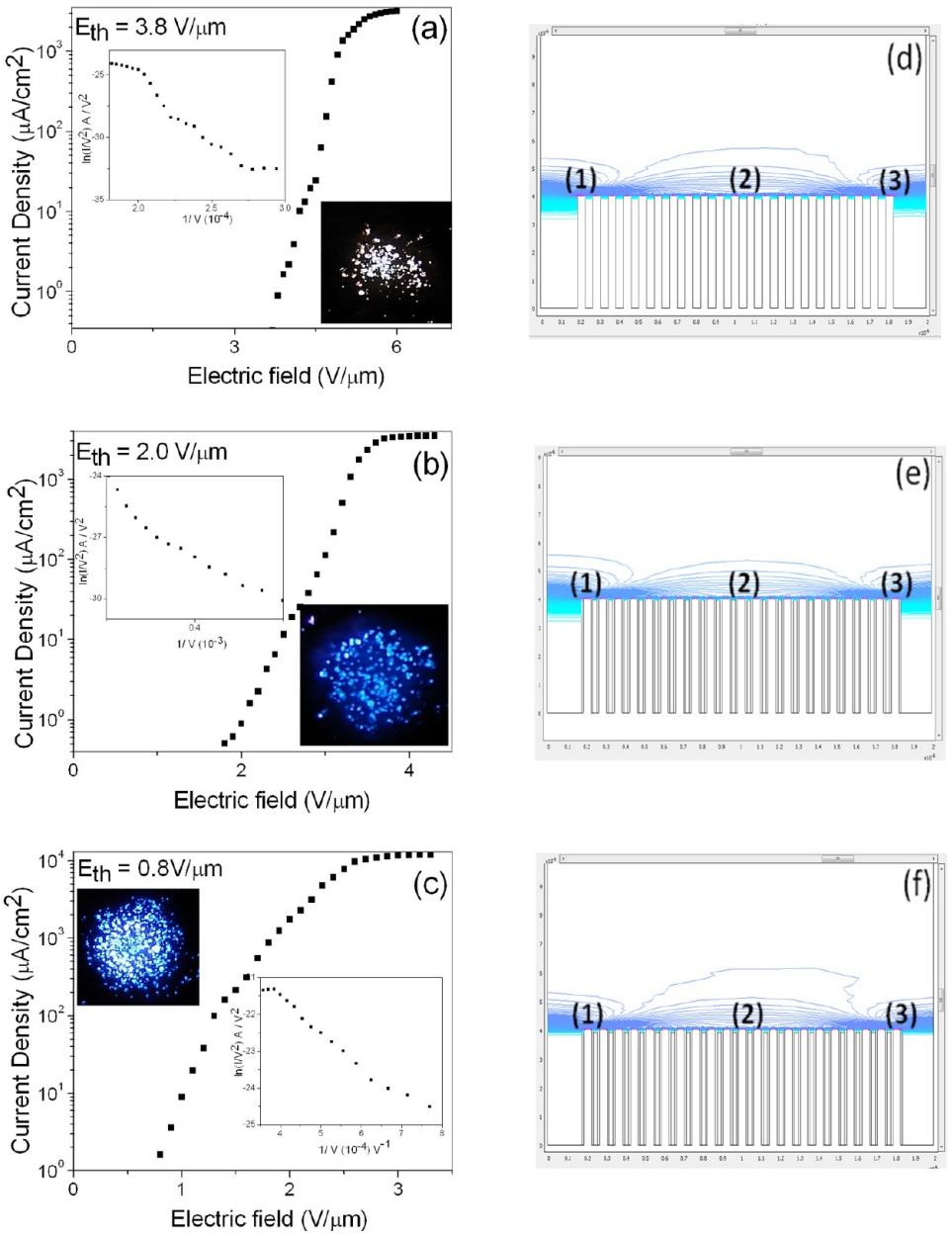

Figure 6. Electron field emission properties (a–c) and the simulated potential maps (d–f) of the as-grown (a,d), STO–CNT (b,e), and PMMA–STO–CNT (c,f) samples.

To further investigate our observation, we have examined the emission site densities as obtained from the fluorescence on the ITO electrode due to electron irradiation. This was performed under a same applied electric field (3.5 V/μm) for all cases. As shown, the emission density for the as-grown sample is poor (inset of Figure 6a). This is due to a screen effect from adjacent CNTs in the CNT forest, consistent with our previous observation.[9] Emission density from the STO–CNT sample (inset of Figure 6b) is higher. This cannot be solely explained by the reduced work function as this will mainly increase the current density from each emitter and not increase the number of emitters in the STO–CNT sample. This means that the $SrTiO_3$ coating has also reduced the screening effect of the CNT forest. Now, let us examine the effect of removing the $SrTiO_3$ coating from the CNT tips. This was done after coating STO–CNT with PMMA. As shown in the inset of Figure 6c, the emission density of the PMMA–STO–CNT matrix is even higher than that of the STO–CNT. This means that the conformal coating of STO–CNT with PMMA followed by the exposure of the CNT tips has increased the number of emitters. In short, the PMMA–STO–CNT matrix offers the lowest E_{th} and the highest emission density. Finally, the actual density would appear to be higher at a distance closer to the sample surface, as the images shown here were collected at an anode–cathode distance of ~1 mm. From the sizes of the sample and the overall fluorescence image, the divergence angle of the emission was estimated as 23.5°.

We have then simulated and compared the local electric field strength at the tips of CNTs for all samples by the COMSOL Multiphysics software. This will allow us to understand the effect of conformal $SrTiO_3$ coating on the whole surface of VA-MWCNTs, as well as the local removal of these $SrTiO_3$ coatings at the tips of the nanotubes. The simulation parameters are as follows: diameter of CNTs, D_{CNTs} = 40 nm; length of CNTs, L_{CNTs} = 4 μm; edge to edge spacing between CNTs, S = 60 nm; applied electric field between top and bottom boundaries, E_{appl} = 5 V/μm. The simulated potential map for an array of as-grown VA-MWCNTs is shown in Figure 6d. As shown, the CNT located at the center of the array (point 2) experienced the highest screening effect from the surrounding nanotubes and thus possesses the lowest electric field ($\sim$9.898 $\times$ 10^6 V/m at point 1, $\sim$5.326 $\times$ 10^6 V/m at point 2, and $\sim$9.97 $\times$ 10^6 V/m at point 3). The effect of $SrTiO_3$ coatings was simulated by setting the spaces next to the surfaces of each CNT (20 nm thickness) with a dielectric constant $k \sim 475$ (instead of vacuum $k \sim 1$). The potential surfaces for the simulated STO–CNT sample are illustrated in Figure 6e. Again, the CNT at the center (point 2) experienced the largest screening effect and lowest local field ($\sim$8.878 $\times$ 10^6 V/m at point 2). This local field is increased by $\sim$66.7% as compared to that in the as-grown sample. The local fields at the tips of CNTs located at the edges of the array are also increased (as high as $\sim$1.559 $\times$ 10^7 V/m at point 1 and point 3). These are due to the reduced screening effect as the "vacuum" surrounding the CNTs is now partially replaced by "$SrTiO_3$ coatings" that have a much higher dielectric constant. Simulation for the PMMA–STO–CNT matrices was conducted by setting the remaining vacuum spacing between the STO–CNT with PMMA coatings (dielectric constant, k = 3.4).[12] In this case, only the sides of the CNTs are simulated with the $SrTiO_3$ and PMMA coatings but not at the top surface of the nanotube tips. This is consistent with the opened-tip configuration of the matrices. As shown in Figure 6f, the local field at the center of the PMMA–STO–CNT matrix ($\sim$9.366 $\times$ 10^6 V/m at point 2) is now $\sim$75.9% higher than that in the as-grown sample due to the additional PMMA filling. The local fields at the edges of the matrix are as high as $\sim$1.298 $\times$ 10^7 V/m at point 1 and point 3.

From these simulations, it is obvious that $SrTiO_3$ coating can reduce the screening effects and enhance the local field by $\sim$66.7% at areas where MWCNTs are closely packed (points 2). Consequently, the reduced screening effect has the contribution toward lower E_{th} and higher emission site density of the STO–CNT sample detected here. However, the additional filling of PMMA did not further enhance the local field by much ($\sim$75.9% instead of $\sim$66.7%) for the fully filled PMMA–STO–CNT matrices. This is expected since the dielectric constant of PMMA is 2 orders of magnitude smaller than that of $SrTiO_3$, while their thicknesses on the PMMA–STO–CNT sample are similar. In fact, there is one factor which was not considered in the simulation, that is, the effect of work function (Φ) on the tunneling process. Coatings of wide band gap materials were in the past claimed to reduce the work function of CNTs and allow easier electron field emission.[13–16] However, Tanaka *et al.* proposed that an insulator (amorphous carbon film) can form an insulating barrier on individual CNTs and increase the Φ and the E_{th}.[23] If this is true, the removal of PMMA and $SrTiO_3$ coatings from the tips of CNTs in our PMMA–STO– NT matrices will remove the insulating barrier while reducing the screening effects by coating PMMA and $SrTiO_3$ at spaces between CNTs. This means that $SrTiO_3$ coatings on our STO–CNT sample improve the performance of CNTs by reducing the screening effect more than the retarding effect of forming an insulating barrier. The exposure of the CNT tips thereafter retains the reduced screening effect and removes the barrier layer. This interpretation is consistent with our simulation that the screening effects (and local fields) at points 2 in both the STO–CNT sample and PMMA–STO–CNT matrix are quite similar. The actual enhancement factor of the matrix is the removal of the insulating barrier. Of course, we cannot totally rule out the possibility that very thin $SrTiO_3$ coatings may still remain at the CNT tips. Since such coating is thin, the added potential barrier is thin and still allows effective band bending and tunneling process.

Thus, we have seemingly explained all of the experimental results. However, we think that the simulated local field enhancement is moderate and there may be other factors behind the experimental observation. We have further interpreted our results with the following model. In this model, we are considering a MWCNT with distances r_i from adjacent nanotubes (i = 1, 2, 3,...). The electric field imposed on an electron located in this nanotube by other electrons located at adjacent MWCNTs is given by

$$E \approx \left(\frac{q}{4\pi\varepsilon_0}\right)\left(\frac{1}{r_1^2}+\frac{1}{r_2^2}+\frac{1}{r_3^2}+....\right) \quad (1)$$

where ε_0 is the permittivity of vacuum and q is the charge of electrons. When the spacing between these MWCNTs is filled by materials with a dielectric constant k, the electric field E will become E'

$$E' \approx \left(\frac{q}{4\pi\varepsilon_0 k}\right)\left(\frac{1}{r_1^2}+\frac{1}{r_2^2}+\frac{1}{r_3^2}+....\right) \quad (2)$$

Hence the electric field imposed on this particular electron is reduced by the factor of k. In principle, if we fill up the spaces between VA-MWCNTs by $SrTiO_3$, Coulomb repulsion forces between electrons located at adjacent CNTs in such a STO–CNT sample will be reduced by a factor as high as 475-fold.

Assuming that such a fully filled STO–CNT sample exists, electron flows on CNTs during field emission can be represented by Figure 7a,b. In the current model, electron flows along CNTs are driven by the electric forces (F_E) generated by the applied electric field between the anode and the cathode. In addition, we assume that Coulombic repulsion forces, F_e (=qE, E = electric field in eq 1), are generated by electrons in the neighboring CNTs in directions different to the driving force F_E. This means that electrons will not simply transport from the cathode to the anode (upward) but will be drifted left and right on the graphene sheets of the nanotubes due to the surrounding Coulombic forces (Figure 7a). In the case of a fully filled STO–CNT sample, the drifting will be smaller due to the smaller repulsion forces F_e' (=eE', E' = electric field in eq 2).

Let us consider the effective path length traveled by electrons under different Coulomb repulsion forces. Practically, CNTs on the same sample will have different lengths, diameters, and thus resistance. The effective applied field on each CNT will be different and lead to different electron flow rates and electron densities. Let us consider a model with three adjacent electrons (e_1, e_2, and e_3) on three CNTs with slightly different lengths, as shown in Figure 7a. Due to different electron flow rates, these three electrons will be located at different distances from the cathode at this particular instant. The second electron (e_2) will be affected by Coulomb repulsion forces F_{1-2} imposed by e_1 and F_{3-2} imposed by e_3 located at r_{1-2} and r_{3-2} away, respectively. Since $r_{3-2} < r_{1-2}$, $|F_{3-2}| > |F_{1-2}|$, this will lead to an effective Coulomb repulsion force F_e that will drift e_2 to the left. Since the current densities in these CNTs are different, the locations and number of electrons surrounding e_2 will be changing with time. The effective F_e will also be changing with time and continuously drifts e_2 away from the direction of F_E and result in a drifting path toward the anode as shown. For the same set of CNTs located in a fully filled STO–CNT sample (Figure 7b), all of the Coulomb

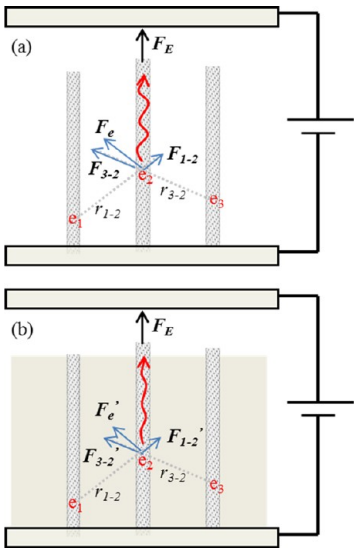

Figure 7. Schematic of electron flows in (a) as-grown sample and (b) fully filled STO–CNT sample.

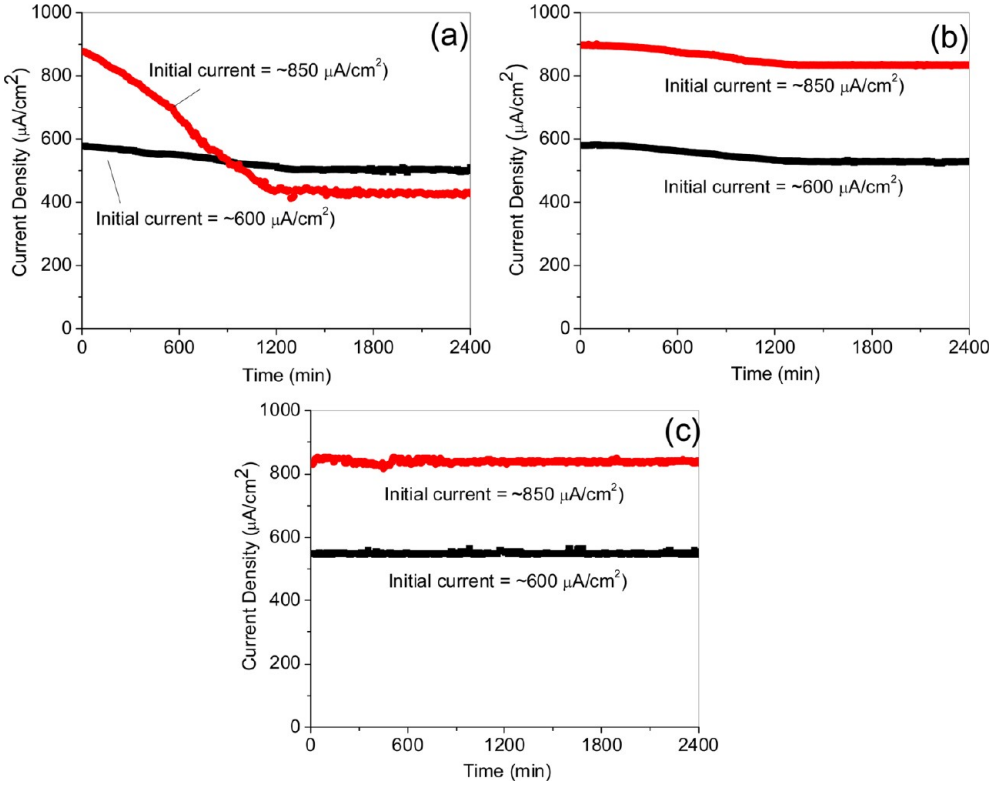

Figure 8. Emission current stability curves for (a) as-grown, (b) STO–CNT sample, and (c) PMMA–STO–CNT matrix.

repulsion forces will be reduced to F_{3-2}', F_{1-2}', and F_e'. Since $|F_e'| < |F_e|$, e_2 will now be drifted less and lead to a shortened propagation path, as shown in Figure 7b.

In practice, CNTs are not defect-free. This means that electron flows along MWCNTs will be scattered by defects and generate Joule heating. Due to the shorter effective path length traveled by electrons, Joule heating in a fully filled STO–CNT sample is lower compared to the case for an as-grown sample. As reported in our earlier papers, electron scattering and Joule heating are responsible for poor emission stability.[8,9] In fact, we have attempted to fully fill up the spaces between CNTs by $SrTiO_3$ coatings. However, thicker $SrTiO_3$ coating results in brittle and void structures and cannot be used for our experiments. We have thus filled up the spaces in our STO–CNT sample with PMMA, which has enabled the tip removal experiments described so far. According to our model, the coating of $SrTiO_3$ in the STO–CNT samples and the PMMA–STO–CNT matrices can reduce electron scattering and Joule heating and thus are expected to emit electrons with high stability.

In order to verify the above-mentioned hypothesis, we have evaluated the emission stability of our samples. Figure 8a–c shows the changes of emission current density with time for the as-grown sample, STO–CNT sample, and PMM–STO–CNT matrix, respectively. All samples were tested with two different initial current densities (~600 and ~850 $\mu A/cm^2$). As shown in Figure 8a, the emitted current from the as-grown sample was degraded with time, especially at higher tested current density. The STO–CNT sample shows very stable emission current with time, ~5–8% degradation after the continuous 2400 min testing (Figure 8b). The PMMA–STO–CNT matrix shows remarkable emission stability without significant degradation after the continuous 40 h test (Figure 8c). Apparently, the improved emission stability from the STO–CNT sample is as expected from our model. The reduced screening effects in the sample lead to shorter electron diffusion length on VA-MWCNTs and thus reduce the potential Joule heating. Further improvement in emission stability from the PMMA–STO–CNT matrix is explained by further reduction of the screening effect from the PMMA filling and the removal of the insulating barrier at the tips of the VA-MWCNTs.

CONCLUSION

Field emission properties of the as-grown VA-MWCNTs were improved due to the reduced screening effect between CNTs after the coating of $SrTiO_3$ which has a high dielectric constant. Such an enhancement can be further improved by the removal of the insulating barrier at the tips of the nanotubes by forming the opened-tip PMMA–STO–CNT matrices. The field emission threshold electric field decreased from 3.8 V/μm in the as-grown sample to ~0.8 V/μm for the PMMA–STO–CNT samples. This improvement is also much better than what we have reported from PMMA–CNT matrices.[24] We propose that the coating of dielectrics ($SrTiO_3$ and PMMA) could have also reduced the Coulomb repulsion forces between electrons in neighboring CNTs. This has led to lower drifting of electron flows in CNTs and thus reduced electron–phonon scattering and Joule heating. Such a shorter effective transport distance of the electrons in CNTs helps improve the emission stability as proven later experimentally.

Finally, we are interested in employing CNTs with better crystallinity to form PMMA–STO–CNT matrices. As we have previously demonstrated,[8] better nanotube crystallinity reduced Joule heating and led to improved stability and enhanced emission current density. This is also consistent with recent works on emission stability using high-quality single-walled CNT loops,[25] CNT yarns,[26] CNT pillars,[27] and CNT composite bundles.[28] The major challenges will be to fabricate large arrays of these CNTs on substrates, followed by the coating of $SrTiO_3$, and the filling of PMMA without distorting the vertical alignment of these highly crystalline CNTs with very high aspect ratios. If these issues are resolved, very high performance and stable field emission displays would be realized in the future.

METHODS

Our VA-MWCNTs were prepared by a dual RF-plasma-enhanced chemical vapor deposition technique.[17] In brief, Ni films (10 nm thick) were first deposited on p^{++} Si substrates (1–10 $\Omega \cdot$cm) by RF magnetron sputtering. These substrates were then used for the growth of VA-MWCNTs at 450 °C by using pure methane gas. Our VA-MWCNTs were grown within a circular area (7 mm in diameter). Three identical samples can be prepared in every growth process. Each set of these samples was used as (1) as-grown VA-MWCNTs, (2) $SrTiO_3$-coated VA-MWCNTs (STO–CNTs), and (3) PMMA–STO–CNT matrices.

The STO–CNT samples were prepared by coating $SrTiO_3$ (10–60 nm thick) on the as-grown VA-MWCNTs by pulsed-laser deposition at room temperature. As shown in Figure 2b, the coating thickness is thicker near the tips of the CNTs and thinner and more uniform on most parts of the CNT side walls. These CNT tips are removed after PMMA filling to form the PMMA–STO–CNT matrices. On the basis of limited TEM study (Figure 3d), the actual thickness on the CNT side walls appears to be thinner than that suggested by the thickness sensor, probably due to the larger CNT surface area than the sensor area. However, accurate coating thickness is difficult to estimate by limited TEM study performed so far and could not be correlated to the thickness measured by the sensor.

The preparation of PMMA–STO–CNT matrices was carried out by dip coating STO–CNT samples by PMMA and followed by mechanical polishing. The PMMA solution was prepared by diluting PMMA with the developer liquid (Microchem) in a volume ratio of 1:1. The STO–CNT samples were dipped into the solution for 15 min and followed by annealing (~100 °C for

2−3 min). The cured samples were then mechanically polished by using fiber-free lapping cloth and a colloidal silica (0.02 μm in diameter) solution to open the tips of the CNTs.

All samples were characterized by field emission scanning electron microscopy (FESEM) and Raman spectroscopy (laser wavelength ~632 nm, laser spot size ~1 μm in diameter under a confocal microscope). The STO−CNT samples were also characterized by transmission electron microscopy (TEM) and X-ray photoelectron spectroscopy (XPS). The monochromatic focused Al Kα X-ray (1486.7 eV) source was used for the XPS measurement. The field emission measurements were conducted in a planar diode configuration at a base vacuum pressure of 10^{-8} mbar.[8,9] The spacing between the anode (indium tin oxide/ITO film on glass) and the tips of the VA-MWCNTs was maintained at 1000 ± 10 μm without using a dielectric spacer. All measurements were reconfirmed by repeating measurements on the same sample as well as additional sets of samples prepared in the same growth process and treatment.

Conflict of Interest: The authors declare no competing financial interest.

Acknowledgment. This work was supported by the Defense Advanced Research Projects Agency (Contract No. DAAD17-03-C-0115 through the U.S. Army Research Laboratory), and the U. S. Department of Army (Grant No. W911NF-04-1-0029 through the City College of New York). Part of the sample characterization was performed at the Environmental Molecular Sciences Laboratory, a national scientific user facility sponsored by the Department of Energy's Office of Biological and Environmental Research located at Pacific Northwest National Laboratory.

REFERENCES AND NOTES

1. de Heer, W. A.; Chatelain, A.; Ugarte, D. A Carbon Nanotube Field-Emission Electron Source. *Science* **1995**, *270*, 1179–1180.
2. Collins, P. G.; Zettl, A. A Simple and Robust Electron Beam Source from Carbon Nanotubes. *Appl. Phys. Lett.* **1996**, *69*, 1969–1971.
3. Choi, W. B.; Chung, D. S.; Kim, H. Y.; Jin, Y. W.; Han, I. T.; Lee, Y. H.; Jung, J. E.; Lee, N. S.; Park, G. S.; Kim, J. M. Fully Sealed, High-Brightness Carbon-Nanotube Field-Emission Displays. *Appl. Phys. Lett.* **1999**, *75*, 3129–3231.
4. Nilsson, L.; Groening, O.; Emmenegger, C.; Kuettel, O.; Schaller, E.; Schlapbach, L.; Kind, H.; Bonard, J. M.; Kern, K. Scanning Field Emission from Patterned Carbon Nanotube Films. *Appl. Phys. Lett.* **2000**, *76*, 2071–2073.
5. Han, I. T.; Kim, H. J.; Park, Y.; Lee, N.; Jang, J. E.; Kim, J. W.; Jung, J. E.; Jong, M. K. Fabrication and Characterization of Gated Field Emitter Arrays with Self-Aligned Carbon Nanotubes Grown by Chemical Vapor Deposition. *Appl. Phys. Lett.* **2002**, *81*, 2070–2072.
6. Bonard, J. M.; Klinke, C.; Dean, K. A.; Coll, B. F. Degradation and Failure of Carbon Nanotube Field Emitters. *Phys. Rev. B* **2003**, *67*, 115406 (1−10).
7. Dean, K. A.; Burgin, T. P.; Chalamala, B. R. Evaporation of Carbon Nanotubes during Electron Field Emission. *Appl. Phys. Lett.* **2001**, *79*, 1873–1875.
8. Kayastha, V. K.; Ulmen, B.; Yap, Y. K. Effect of Graphitic Order on Field Emission Stability of Carbon Nanotubes. *Nanotechnology* **2007**, *18*, 035206-4A.
9. Pandey, A.; Prasad, A.; Moscatello, J.; Ulmen, B.; Yap, Y. K. Enhanced Field Emission Stability and Density Produced by Conical Bundles of Catalyst-Free Carbon Nanotubes. *Carbon* **2010**, *48*, 287–292.
10. Shiraishi, M.; Ata, M. Work Function of Carbon Nanotubes. *Carbon* **2001**, *39*, 1913–1917.
11. Maus-Friedrichs, W.; Frerichs, M.; Gunhold, A.; Krischok, S.; Kempter, V.; Bihlmayer, G. The Characterization of $SrTiO_3$ (001) with MIES UPS (HeI) and First-Principles Calculation. *Surf. Sci.* **2002**, *515*, 499–506.
12. Pontes, F. M.; Lee, E. J. H.; Leite, E. R.; Longo, E.; Varela, J. A. High Dielectric Constant of $SrTiO_3$ Thin Films Prepared by Chemical Process. *J. Mater. Sci.* **2000**, *35*, 4783–4787.
13. Yi, W.; Jeong, T. W.; Yu, S. G.; Heo, J. N.; Lee, C. S.; Lee, J. H.; Kim, W. S.; Yoo, J. B.; Kim, J. M. Field-Emission Characteristics from Wide-Bandgap Material-Coated Carbon Nanotubes. *Adv. Mater.* **2002**, *14*, 1464–1468.
14. Lee, J.; Lee, W.; Sim, K.; Han, S. H.; Yi, W. Improved Field Emission Properties from Polycrystalline Indium Oxide-Coated Single-Walled Carbon Nanotubes. *J. Vac. Sci. Technol., B* **2008**, *26*, 1892–1895.
15. Zhang, J.; Yang, C.; Wang, Y.; Feng, T.; Yu, W.; Jiang, J.; Wang, X.; Liu, X. Improvement of the Field Emission of Carbon Nanotubes by Hafnium Coating and Annealing. *Nanotechnology* **2006**, *17*, 257–260.
16. Jin, F.; Liu, Y.; Day, C. M.; Little, S. A. Enhanced Electron Emission from Functionalized Carbon Nanotubes with a Barium Strontium Oxide Coating Produced by Magnetron Sputtering. *Carbon* **2007**, *45*, 587–593.
17. Menda, J.; Ulmen, B.; Vanga, L. K.; Kayastha, V. K.; Yap, Y. K.; Pan, Z.; Ivanov, I. N.; Puretzky, A. A.; Geohegan, D. B. Structural Control of Vertically Aligned Multiwalled Carbon Nanotubes by Radio-Frequency Plasmas. *Appl. Phys. Lett.* **2005**, *87*, 173106-3.
18. Chakrabarti, S.; Pan, L.; Tanaka, H.; Hokushin, S.; Nakayama, Y. Stable Field Emission Property of Patterned MgO Coated Carbon Nanotube Arrays. *Jpn. J. Appl. Phys.* **2007**, *46*, 4364–4369.
19. Schlesser, R.; McClure, M. T.; McCarson, B. L.; Sitar, Z. Bias Voltage Dependent Field-Emission Energy Distribution Analysis of Wide Band-Gap Field Emitters. *J. Appl. Phys.* **1997**, *82*, 5763–5772.
20. van Benthem, K.; Elsässer, C.; French, R. H. Bulk Electronic Structure of $SrTiO_3$: Experiment and Theory. *J. Appl. Phys.* **2001**, *90*, 6156–6164.
21. Givargizov, E. I.; Zhirnov, V. V.; Stepanova, A. N.; Rakova, E. V.; Kiselev, A. N.; Plekhanov, P. S. Microstructure and Field Emission of Diamond Particles on Silicon Tips. *Appl. Surf. Sci.* **1995**, *87/88*, 24–30.
22. Fowler, R. H.; Nordheim, L. Electron Emission in Intense Electric Fields. *Proc. R. Soc. A* **1928**, *119*, 173–181.
23. Tanaka, H.; Akita, S.; Pan, L.; Nakayama, Y. Barrier Effect on Field Emission from Stand-Alone Carbon Nanotube. *Jpn. J. Appl. Phys.* **2004**, *43*, 864–867.
24. Pandey, A.; Prasad, A.; Moscatello, J.; Yap, Y. K. Stable Electron Field Emission from PMMA−CNT Matrices. *ACS Nano* **2010**, *4*, 6760–6766.
25. Futaba, D. N.; Kimura, H.; Zhao, B.; Yamada, T.; Kurachi, H.; Uemura, S.; Hata, K. Carbon Nanotube Loop Arrays for Low-Operational Power, High Uniformity Field Emission with Long-Term Stability. *Carbon* **2012**, *50*, 2796–2803.
26. Lee, J.; Jung, Y.; Song, J.; Kim, J. S.; Lee, G. W.; Jeong, H. J.; Jeong, Y. High-Performance Field Emission from a Carbon Nanotube Carpet. *Carbon* **2012**, *50*, 3889–3896.
27. Perea-López, N.; Rebollo-Plata, B.; Briones-León, J. A.; Morelos-Gómez, A.; Hernández-Cruz, D.; Hirata, G. A.; Meunier, V.; Bottello-Méndez, A. R.; Charlier, J.-C.; Maruyama, B.; *et al.* Millimeter-Long Carbon Nanotubes: Outstanding Electron-Emitting Sources. *ACS Nano* **2011**, *5*, 5072–5077.
28. Kim, W. J.; Lee, J. S.; Lee, S. M.; Song, K. Y.; Chu, C. N.; Kim, Y. H. Better than 10 mA Field Emission from an Isolated Structure Emitter of a Metal Oxide/CNT Composite. *ACS Nano* **2011**, *5*, 429–435.